The Influence of Precipitated Austenite on Hydrogen Embrittlement in 5.5Ni Steel

Y.-H. KIM, H. J. KIM, and J. W. MORRIS, Jr.

This work was undertaken to test the influence of precipitated austenite on transgranular hydrogen embrittlement in 5.5Ni steel. Prior work has shown that the mechanism of transgranular hydrogen embrittlement in this steel is interlath separation. Since the austenite that forms during the tempering of 5.5Ni steel precipitates on the martenite lath boundaries, it was hypothesized that the austenite might have a beneficial effect. The experimental results show, however, that the precipitated austenite decreases the toughness in the presence of hydrogen. The apparent mechanism is straightforward. The precipitated austenite transforms to martensite in the strain field ahead of the crack tip. Interlath cracks appear at the periphery of the fresh martensite particles. They are apparently caused by the volume change that accompanies the martensite transformation, which imposes a tension across the lath boundary. The interlath cracks link together to form the macroscopic fracture.

I. INTRODUCTION

SEVERAL investigators[1-4] have suggested that retained austenite is beneficial to the hydrogen resistance of lath martensitic steels. The mechanism of the improvement is, however, unclear, and there are indications from other work that the austenite may be harmful.[5] To help clarify this issue it was decided to investigate hydrogen embrittlement in an alloy whose microstructure and fracture modes are well understood.

The alloy selected was a commercial 5.5Ni steel manufactured by the Nippon Steel Corporation. This alloy was developed for structural use at cryogenic temperature, and is toughened for cryogenic service by a three-step heat treatment (called the QLT treatment)[6,7] that causes the precipitation of a significant amount of a thermally stable austenite along martensite lath boundaries. The morphology, composition, and mechanical behavior of this precipitated austenite have been studied in detail.[6-11]

The mechanism of hydrogen embrittlement in commercial 5.5Ni steel is also known.[12] When the alloy is tested in the tempered condition in the presence of hydrogen, it fractures by decohesion along the martensite lath boundaries.

The plan of the present work was to use heat treatment to introduce a controlled distribution of precipitated austenite along the martensite lath boundaries and determine the influence of this austenite on the degree and mechanism of hydrogen embrittlement. Since the intercritical tempering treatments that introduce austenite in this steel also temper the dislocated lath martensite matrix, two heat treatments were used. The first, designated QT, provides a tempered martensite with very little precipitated austenite. This was the heat treatment studied in Reference 12. The second, the QLT treatment, provides a tempered martensite matrix that is densely decorated with fine interlath islands of austenite.

Y.-H. KIM is Research Scientist with T. J. Watson Research Center, IBM, P.O. Box 218, Yorktown Heights, NY 10598. H. J. KIM is Research Scientist with Welding Research Institute, Hyundai Heavy Ind. Co., Ltd., 1, Cheonha-dong, Ulsan, Korea. J. W. MORRIS, Jr., is Professor of Metallurgy, University of California, Berkeley, 278 Hearst Mining Building, Berkeley, CA 94720.

Manuscript submitted November 13, 1984.

II. EXPERIMENTAL PROCEDURE

The alloy used for this work was a commercial 5.5Ni steel made by the Nippon Steel Corporation. Its chemical composition is, in weight percent, Fe-5.86Ni-1.21Mn-0.69Cr-0.20Mo-0.20Si-0.06C-0.01S-0.008P. The alloy was supplied as a 35 mm plate in the QLT condition.

The alloy was annealed at 1200 °C for 2 hours to remove the effects of prior thermomechanical treatments, austenitized at 800 °C for 1 hour, and quenched in ice water to room temperature. Samples cut from the plate were then given one of two heat treatments. The first was an intercritical temper for 1 hour at 600 °C to produce the condition designated QT. The second was the conventional QLT treatment: an intercritical anneal for 1 hour at 670 °C followed by an intercritical temper for 1 hour at 600 °C.

The microstructures were studied with optical, scanning, and transmission electron microscopy. The foils used for transmission electron microscopy were thinned by electropolishing in a solution of 400 ml CH_3COOH, 75 mg Cr_2O_3, and 21 ml H_2O.[13]

The volume fraction of precipitated austenite was determined by X-ray diffraction using Miller's method,[14] in which the average integrated intensities of the (220) and (311) austenite peaks are compared to that of the (211) martensite peak. The specimen surface was prepared for X-ray diffraction by grinding with up to 600 grade emery paper, followed by etching for 10 minutes in a solution containing 3 ml HF + 100 ml 30 pct H_2O_2.

Specimens for mechanical testing were machined from the heat-treated plate. ASTM standard round bar tensile specimens with 6.35 mm diameter were used for the tensile tests. Standard Charpy v-notch specimens were prepared and fatigue precracked for fracture toughness tests in three-point bending.

Hydrogen was introduced into the specimens by cathodic charging in a 1 N H_2SO_4 solution. Small amounts of As_2O_3 and CS_2 were added to the electrolyte to prevent hydrogen gas recombination.[12,15] The specimens were charged for 24 hours at various current densities from 10 A/m^2 to 1000 A/m^2.

Tensile and fracture toughness tests were performed on the charged specimens in room temperature air. The tensile tests were started within 5 minutes of the completion of

hydrogen charging and employed a crosshead speed of 6.35×10^{-3} mm/sec. The three-point-bend fracture tests were begun within 2 minutes of the completion of charging.

The fracture surfaces and cross sections through the fracture surface were examined in the optical and scanning electron microscopes, and were also studied by transmission electron microscopy using profile fractographic techniques.[12,16,17] To accomplish the latter the fracture surface was plated with either nickel or pure iron. A thin section perpendicular to the fracture surface was then cut out and thinned until a region containing a portion of the fracture surface was transparent to the 100 kV electron beam.

III. RESULTS

A. *The Starting Microstructure*

When 5.5Ni steel is quenched from the austenite phase, it transforms into lath martensite.[10,13] The dislocated martensite laths are organized into packets. With rare exceptions the laths within a packet are separated by low-angle grain boundaries and share common crystallographic axes. The lath boundaries tend to lie along {110} planes, although they are wavy and occasionally dovetail into one another. The packet boundaries and the prior austenite grain boundaries are irregular, high-angle boundaries.

When the alloy is tempered at a temperature just within the two-phase $\alpha + \gamma$ field, as it is in the QT heat treatment, the dislocation network within the martensite is partly recovered and austenite is precipitated along the martensite lath boundaries.[9,10] The microstructure of the QT alloy is shown in Figure 1. The volume fraction of precipitated austenite is only 1.8 pct, reflecting the relatively low tempering temperature and short tempering time.

The three-step QLT treatment produces a highly tempered martensite structure with a dense distribution of precipitated austenite.[9,10] The microstructure is shown in Figure 2. The tempered martensite laths are outlined by well-defined boundaries even though the alloy has been tempered twice. The precipitated austenite content is about 8.5 vol pct. The dark-field micrograph in Figure 2(b) brings out the elongated austenite particles along the martensite lath boundaries. Since the lath boundaries are very low-angle boundaries, it is possible for the interlath austenite to be simultaneously in almost exact crystallographic registry with both of the neighboring martensite laths. The Kurdjumov-Sachs (KS) relation[18] is usual, although the Nishiyama-Wasserman (NW) relation[19,20] is also occasionally observed.

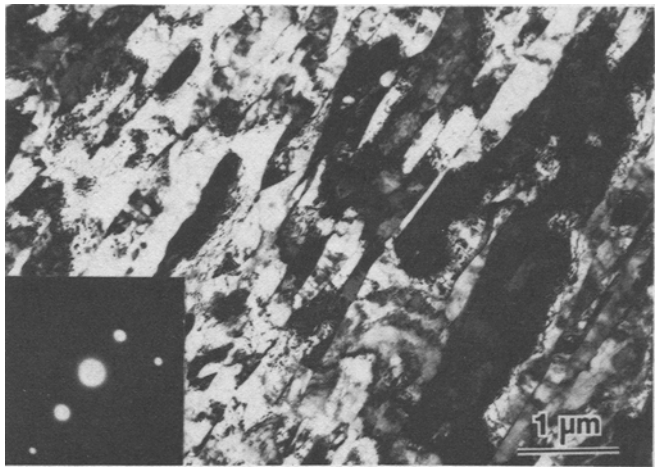

Fig. 1—Transmission electron micrograph showing the microstructure of 5.5Ni steel in the QT condition.

B. *Mechanical Tests*

The results of the uniaxial tensile tests are presented in Table I. In the uncharged condition the QLT specimen has a lower yield and ultimate tensile strength than the QT specimen, but has greater ductility. Both alloys are significantly embrittled by hydrogen charging. The strength increases slightly while the ductility decreases substantially. The QLT specimen is the more severely embrittled of the two. After charging, the QLT specimen has a much lower tensile elongation than the QT specimen (2.2 pct *vs* 5.6 pct) and an ever more obviously depressed reduction in area (2.9 pct *vs* 17.8 pct). This result is significant since the QLT specimen has a lower yield strength, and lower strength usually decreases sensitivity to hydrogen.[4,21]

The results of the three-point bend tests were, qualitatively, the same. Before hydrogen charging, both the QT and QLT alloys had high fracture toughness (330 MPa · $m^{1/2}$ and 360 MPa · $m^{1/2}$, respectively). Both specimens were embrittled by hydrogen charging (Figure 3). Again, the QLT specimen was the more severely affected of the two, based on its load-bearing capacity and crack opening displacement. Its estimated fracture toughness (K_{max}) was 100 MPa · $m^{1/2}$, *vs* 180 MPa · $m^{1/2}$ for the QT specimen.

An additional set of mechanical tests was done to test the reversibility of the hydrogen embrittlement phenomenon. One specimen was tested in the as-received QLT condition. A second, identical specimen was hydrogen-charged and

Table I. Tensile Test Data of 5.5 Ni Steel

		QT		QLT	
		(No H)	(H)	(No H)	(H)
Y.S.	(MPa)	737	757	590	616
U.T.S.	(MPa)	779	758	735	616
R.A.	(pct)	79.2	17.8	79.7	2.9
Total elong.*	(pct)	29.8	5.6	34.6	2.2

*25.4 mm (1 inch) gauge length

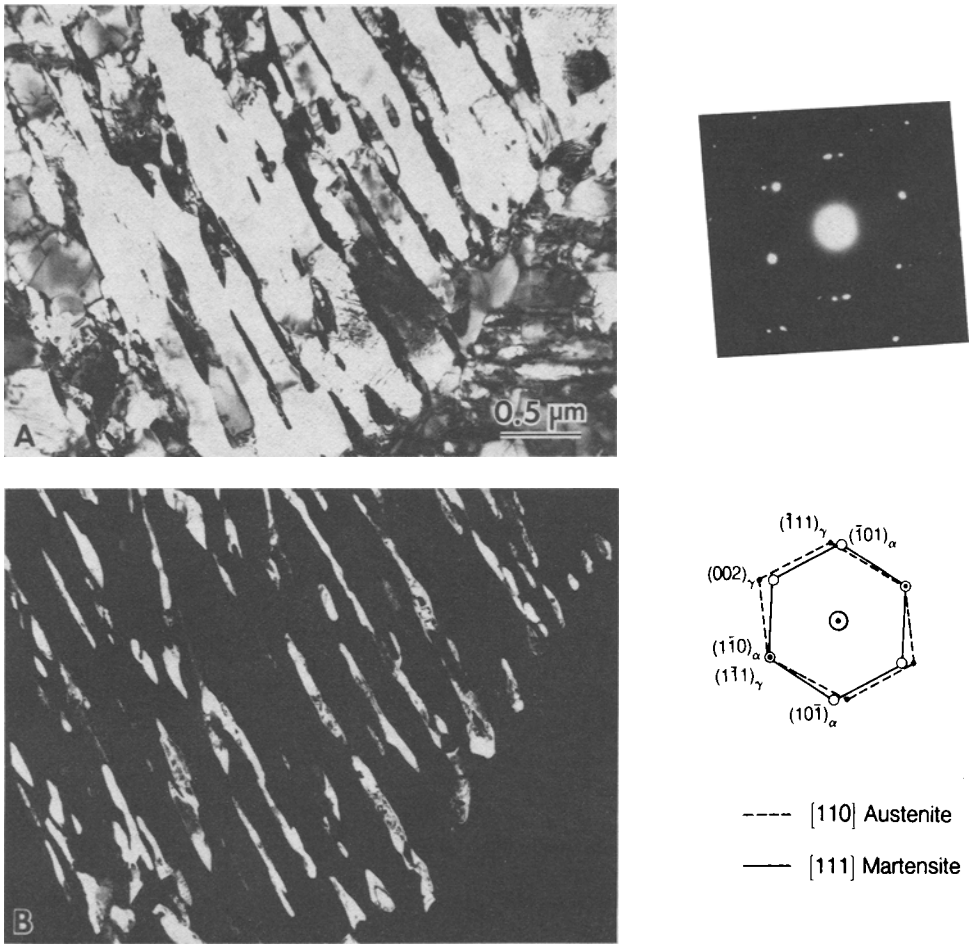

Fig. 2—Transmission electron micrographs showing the microstructure of 5.5Ni steel in the QLT condition. Figure B is a dark-field micrograph taken from a γ diffraction spot, showing precipitated austenite along the martensite lath boundaries.

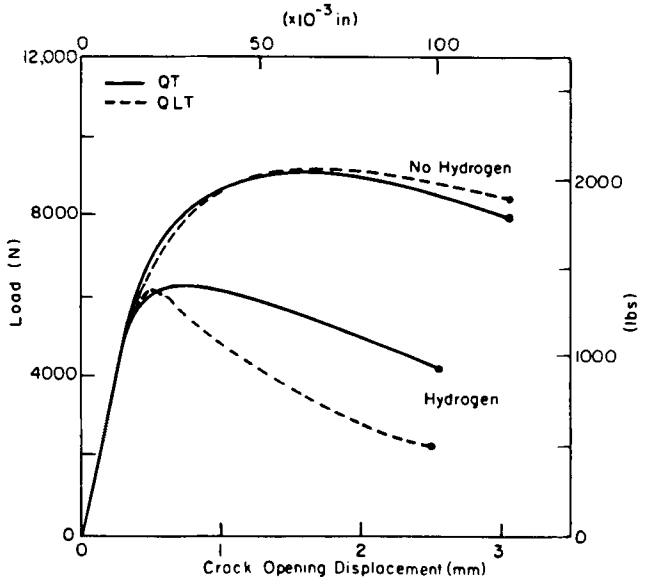

Fig. 3—Load *vs* crack opening displacement for three-point bending tests on the QT and QLT alloys before and after hydrogen charging.

Table II. Degassing Experiment Data

		(No H)	(Baked)
Y.S.	(MPa)	600	604
U.T.S.	(MPa)	751	749
R.A.	(pct)	79.5	78.7
Total elong.*	(pct)	29.9	29.1

*25.4 mm (1 inch) gauge length

then degassed in vacuum at room temperature for thirty days. The mechanical properties of the two specimens are compared in Table II, and are the same to within normal experimental scatter. The result appears to show that the embrittlement is reversible.

C. *Fractographic Analysis*

Without hydrogen charging, both specimens fractured in a fully ductile mode. With charging, both fractured in a mixed mode that included transgranular brittle fracture and dimple rupture (Figure 4). Intergranular fracture (*i.e.*, fracture along the prior austenite grain boundaries) was not observed.

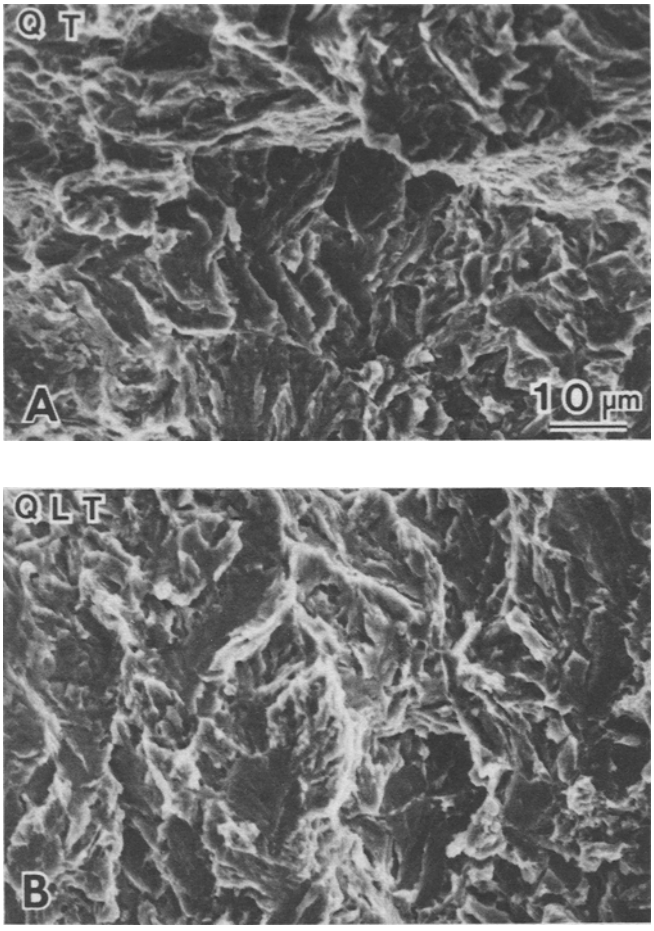

Fig. 4 — Scanning electron fractographs showing the fracture surfaces of the QT and QLT specimens after hydrogen charging and fracture in three-point bending.

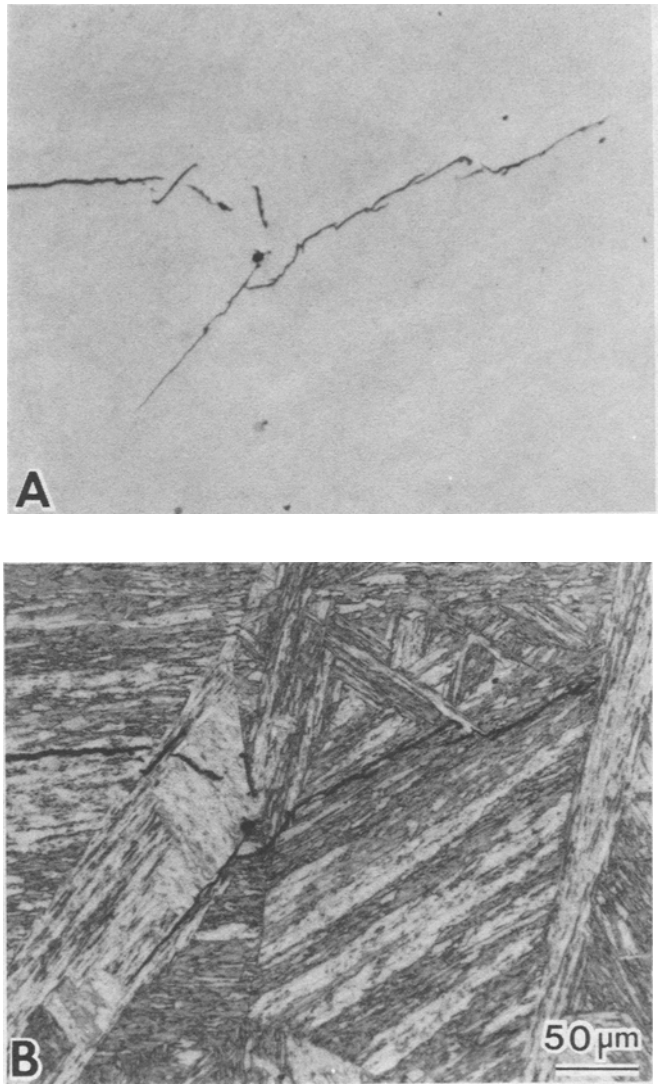

Fig. 5 — Optical micrographs of a plane perpendicular to the fracture surface in a hydrogen-charged specimen, showing secondary cracks ahead of the tip of an arrested crack. Photograph B was taken after etching with nital to reveal the sample microstructure.

Detailed fractographic studies showed that the transgranular brittle fracture in both the QT and QLT specimens was predominantly along the lath boundaries.

Figure 5 shows a section through an untempered specimen that was loaded after hydrogen charging to initiate fracture, then unloaded before the crack had propagated through the whole cross section. (All of the specimens used for high resolution fractography were loaded in three-point bending.) Discrete cracks were found ahead of the arrested macrocrack. Figure 5(a) was taken before chemical etching to show the pattern of the discrete cracks. Figure 5(b) was taken after etching with a 2 pct nital solution to reveal the martensite substructure. This figure shows cracks along the lath boundaries, most of which terminate at packet boundaries. The only translath cracks observed were short crack segments connecting cracks along adjacent lath boundaries. Figure 6 shows a second example of a discrete crack in this sample and illustrates the continuation of interlath cracks across packet boundaries. These observations confirm and complement the profile fractographic data on the QT alloy presented in Reference 12.

Figure 7 is a profile transmission electron fractograph of a QLT specimen that was broken after hydrogen charging. The principal fracture follows lath boundaries. Secondary microcracks appear along the lath boundaries beneath the fracture surface. Some examples are marked by the arrows in the figure. The microcracks vary in length, with the smallest being about 0.01 μm. Since microscopic studies showed that the alloy does not contain microcracks after hydrogen charging alone, the interlath cracking must be associated with mechanical strain.

The influence of the austenite phase was studied by examining the microstructure of broken QLT specimens. These studies were particularly concerned with the stability of the austenite phase and the influence of transformed austenite on the crack path.

Previous work[17,22] on tempered Fe-Ni steels showed that precipitated austenite undergoes an essentially complete transformation to martensite in the deformed region near the crack tip. The hydrogen-charged QLT specimens behaved in the same way. While hydrogen charging did not induce transformation by itself, the precipitated austenite within the charged alloys transformed fully to martensite in the highly strained region near the crack. As shown in Figure 7, the

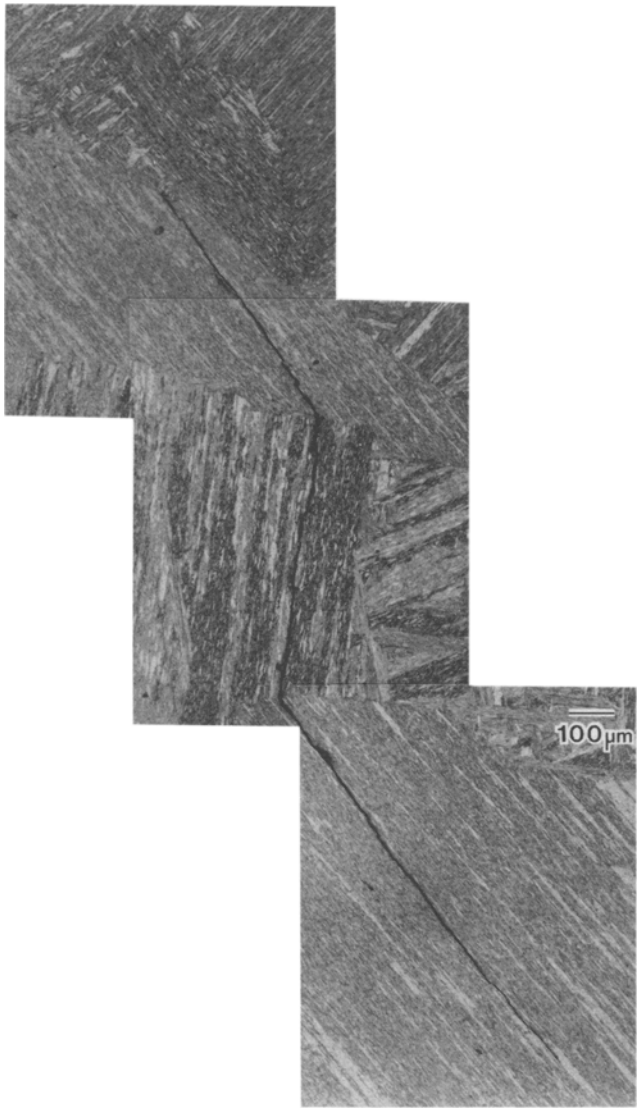

Fig. 6—Optical micrograph of a second etched cross section through the specimen shown in Fig. 5, showing crack propagation along lath boundaries and crack deflection at packet boundaries.

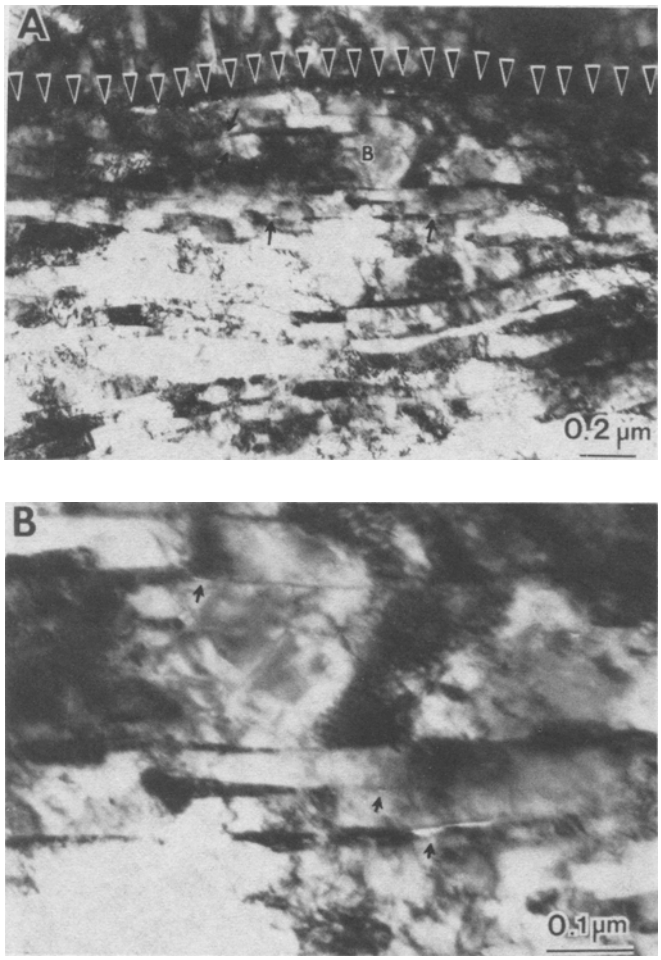

Fig. 7—Transmission electron fractographs of a hydrogen-charged QLT specimen. The fracture surface is marked by the open triangles in micrograph A. The solid arrows point to interlath microcracks just beneath the fracture surface. Micrograph B is a high magnification of the region designated B in micrograph A. The arrows point to interlath microcracks, which tend to lie at the periphery of fresh martensite islands, as evidenced by the cracks at the upper and lower arrows.

regions of the QLT specimens immediately below the fracture surface contain a number of dark interlath islands that are morphologically identical to the precipitated austenite islands shown in Figure 2. Examples are at the ends of the arrows in Figure 7(a), and just to the left of the lowest arrow in Figure 7(b). However, high resolution diffraction studies show that these are dislocated martensite particles. There is an essentially complete transformation of the precipitated austenite near the fracture surface.

There is a striking association between the interlath microcracks and the islands of fresh martensite. The substantial majority of the interlath microcracks emanate from fresh martensite particles. Typical examples are marked by the arrows in Figures 7 and 8.

IV. DISCUSSION

A. *The Mechanism of Hydrogen Embrittlement*

The results presented above show that 5.5Ni steel is susceptible to hydrogen embrittlement when it is in either the QT or QLT conditions. In both cases the fracture path is transgranular and the predominant brittle fracture mode is interlath separation. A dense distribution of small secondary interlath cracks is present near the fracture surface.

These observations are consistent with the mechanism of hydrogen embrittlement that was proposed in Reference 12. Fine cracks form on the lath boundaries ahead of the crack tip and link together to produce macroscopic failure. In both the QT and QLT alloys the lath boundary cracks tend to form at foreign particles in the lath boundary. In the QT alloy the common nucleating particles are interlath carbides, as documented in the profile fractographs presented in Reference 12. In the QLT alloy the predominant nucleation sites are interlath islands of fresh martensite.

B. *The Influence of Retained Austenite*

The results strongly suggest that the presence of precipitated austenite increases the severity of hydrogen embrittlement. The QLT-treated alloy, which has a substantially greater austenite fraction (8.5 pct) than the QT-treated alloy (1.8 pct), is much less tough and ductile after hydrogen charging, even though its yield strength is significantly

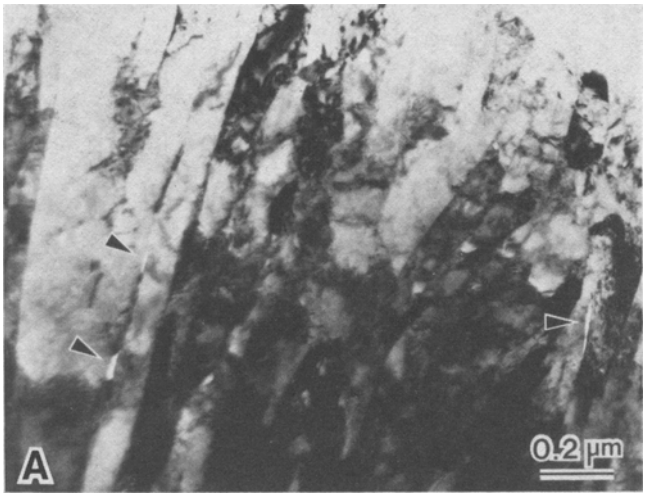

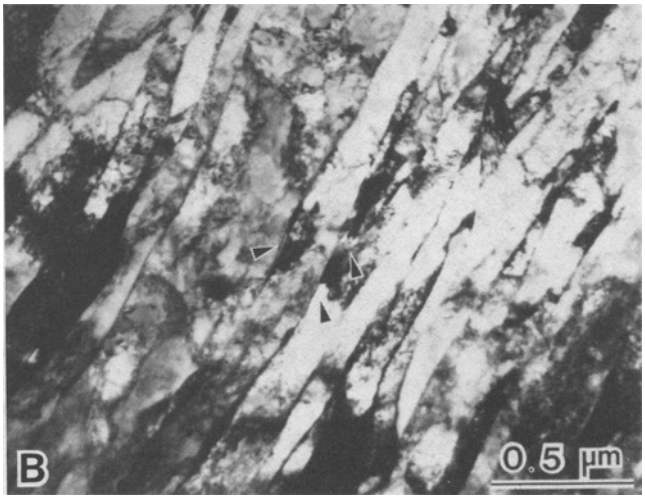

Fig. 8 — Additional transmission electron fractographs of the material immediately below the fracture surface in a hydrogen-charged QLT specimen. The arrows point to interlath microcracks which lie at the edges of fresh martensite particles.

lower and its toughness and ductility in the uncharged condition are higher. Since both alloys have a well-tempered martensite matrix, the principal difference between them is the austenite content.

The conclusion that precipitated austenite is the microstructural flaw in the QLT alloy is reinforced by the fractographic studies. These show that the precipitated austenite near the fracture surface invariably transforms to fresh martensite, and that the interlath cracks that form near the fracture surface almost always appear at the periphery of islands of fresh martensite. The strain-induced martensite transformation provides preferential sites for interlath fracture.

C. *The Mechanism of Embrittlement by Interlath Austenite*

It is intuitively plausible that the transformation of the precipitated austenite islands along the lath boundaries should promote interlath fracture. A possible mechanism is diagrammed in Figure 9.

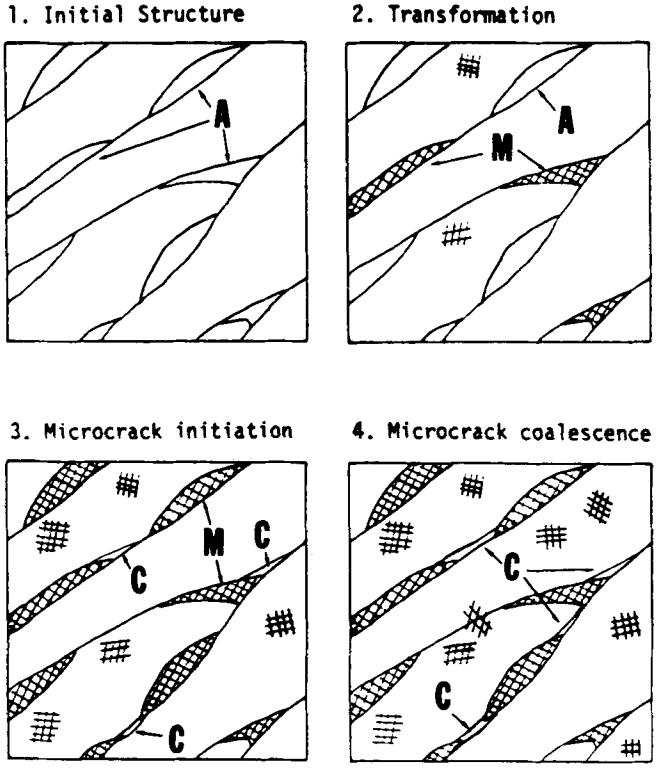

Fig. 9 — Schematic drawing illustrating the probable mechanism of hydrogen embrittlement in the presence of interlath austenite. (1) The initial structure of dislocated martensite with interlath austenite. (2) The interlath martensite transforms to martensite in the stressed region ahead of the crack tip. (3) The transformation volume change imposes a tensile stress across the boundary, which has been weakened by hydrogen, and nucleates microcracks. (4) The microcracks grow and coalesce into macrocracks.

The martensite transformation of the precipitated austenite involves a volume increase of 2 to 3 pct. When the transforming particle is an elongated inclusion that lies in the lath boundary, as it is in the present case, the volume increase must impose a tensile stress perpendicular to the boundary that promotes fracture in the lath boundary plane.

But the volume change on transformation does not cause interlath cracking by itself. The interlath austenite also transforms during the fracture of ferritic steels that are not hydrogen-charged, but does not cause any noticeable fracture on the lath boundaries.[17] In fact, the precipitated austenite is intentionally introduced into these steels to improve their resistance to brittle fracture. However, hydrogen weakens the lath boundaries, as evidenced by the fact that the hydrogen-induced fracture is interlath whether or not austenite is present, to the point where they apparently cannot resist the combination of the external stress and the stress imposed by the martensite transformation.

The transformation of the interlath austenite may actually contribute to the weakness of the lath boundary. Hydrogen is more soluble in the face-centered cubic austenite than in the body-centered cubic ferrite, and has been shown to accumulate in the austenitic constituent of a two-phase alloy.[5] If a saturated interlath austenite transforms, it produces a supersaturated martensite. The most likely hydrogen diffusion path to relieve the supersaturation is along the lath boundary, which should yield a transient increase in the local boundary concentration of hydrogen.

D. *Comparison with Prior Work*

As described in the Introduction, prior work on the influence of retained austenite on hydrogen embrittlement produced mixed results. Some authors[1–4] report an improvement in hydrogen resistance when retained austenite is present while others report a deterioration.[5] Since the fractographic details of the embrittlement are not identified in the papers, it is not possible to give a specific comparison between that work and this. It does seem likely that the embrittlement phenomena reported by Toy and Phillips[5] are similar to those documented here.

It is, moreover, possible to suggest at least two circumstances in which retained austenite might enhance hydrogen resistance. The first was proposed by Ritchie, *et al.*[1] and by Gooch[2] to explain an increased resistance to hydrogen under dynamic conditions. They noted the higher solubility and lower diffusivity of hydrogen in the austenite phase, and suggested that the austenite might act as a sink for hydrogen to retard its migration to the crack front. This model presumes, of course, that the alloy is unsaturated and the austenite is mechanically stable.

The second case in which one would expect the austenite to improve hydrogen resistance is when the alloy is brittle in an intergranular mode in the uncharged condition. Intergranular embrittlement suggests the presence of contaminants on the prior austenite grain boundaries. It is well known that austenite can getter species that promote intergranular attack. It may, therefore, reduce susceptibility to hydrogen relative to that which the alloy would have if its boundaries remained contaminated. The fractographic evidence for this mechanism would be a relative improvement in the toughness in the hydrogen-charged condition accompanied by a change in the fracture mode from intergranular to transgranular. The toughness in the presence of hydrogen would, however, remain less than it would be if both the austenite and the grain boundary contaminant were absent.

E. *The Contrasting Influence of Precipitated Austenite on the Ductile-Brittle Transition*

The QLT treatment was developed for 5.5Ni steel to decrease its ductile-brittle transition temperature for low-temperature service.[6,7] Roughly similar heat treatments are used to control the ductile-brittle transition in other ferritic steels.[8,17,23] The mechanism of brittle fracture in these alloys is transgranular cleavage. The addition of precipitated austenite has the paradoxical effect that it suppresses transgranular thermal embrittlement while it promotes transgranular hydrogen embrittlement.

The source of the paradox lies in the different fractographic mechanisms of transgranular thermal and hydrogen embrittlement. The low-temperature fracture plane is the {100} cleavage plane.[8,10,16] This plane crosses the low-angle martensite lath boundaries with the consequence that martensite packets cleave as a unit. Interlath austenite cuts through the cleavage planes. As described in detail elsewhere,[8,10] the transformation of that austenite subdivides the cleavage planes and decreases the effective grain size. However, hydrogen embrittlement shifts the dominant fracture plane to the lath boundary, which tends to lie near {110}. The interlath austenite lies in these planes. Its transformation promotes interlath fracture by the mechanism outlined above.

F. *Suppressing Transgranular Hydrogen Embrittlement*

Given that the mechanism of transgranular hydrogen embrittlement is interlath separation, there are three ways in which it might be suppressed: (1) by preventing the accumulation of hydrogen in the lath boundaries, (2) by improving the inherent resistance of the lath boundary to hydrogen embrittlement, and (3) by decreasing the mean free path of a lath boundary crack.

It is not clear how either of the first two can be accomplished. The lath boundary will eventually saturate with hydrogen if the specimen is charged. The resistance of the boundary might be improved by eliminating other deleterious chemical species that accumulate there, but the auger spectroscopic studies done to date (in unpublished work in this laboratory) do not reveal any contaminant on the boundary. It is also unclear how desirable species could be induced to condense on the lath boundary, or how the internal structure of the boundary could be changed to improve its inherent resistance.

The microstructural feature that can be controlled, albeit with difficulty, is the dimension of the lath that determines the mean free crack length. Parallel work to this[24] has shown that the lath size is dramatically reduced and the laths have a more equiaxed shape if the alloy is given a repeated rapid thermal cycle that induces a rapid reversion to austenite and retransformation to martensite. As expected, this thermal treatment dramatically improves the hydrogen resistance of lath martensitic steel, just as it dramatically lowers the ductile-brittle transition for thermal embrittlement. This kind of thermal cycle is naturally imposed during the multipass gas-tungsten-arc (GTA) welding of ferritic steels, and may help to explain the improved hydrogen resistance of HY130 welds that are made with a multipass GTA process.[25]

V. CONCLUSION

The present work shows that the hydrogen resistance of 5.5Ni steel decreases when it is heat treated to introduce a dense distribution of precipitated austenite along the lath boundaries of its dislocated lath martensitic substructure. The hydrogen-induced fracture is transgranular, and follows the lath boundaries. The precipitated austenite undergoes a strain-induced transformation to martensite ahead of the crack tip. The strain associated with the transformation, particularly the volume increase, apparently imposes a tensile stress across the lath boundary that promotes fracture. Small microcracks are often found that emanate from the periphery of the transformed austenite particles along the lath boundaries. The transformed austenite may also act as a source of hydrogen that contributes to the embrittlement of the lath boundaries.

It follows that austenite precipitation is not useful for improving resistance to transgranular hydrogen embrittlement in these steels. However, other evidence suggests that retained austenite may help reduce intergranular embrittlement in alloys that have contaminants on the prior austenite grain boundaries. Still other work shows that the resistance to transgranular hydrogen embrittlement is raised by rapid thermal cycling treatments that refine the martensite lath size and decrease the mean free path of an interlath crack.

ACKNOWLEDGMENTS

The authors are grateful to the Nippon Steel Corporation for providing samples of 5.5Ni steel, and to Dr. B. Fultz and M. Strum, Lawrence Berkeley Laboratory, for helpful discussions. This research was supported by the Office of Naval Research under Contract No. N00014-75-C-0154.

REFERENCES

1. R. O. Ritchie, M. Castro-Cedeno, V. F. Zackay, and E. R. Parker: *Metall. Trans. A*, 1978, vol. 9A, p. 35.
2. T. G. Gooch: *Weld. J.*, 1974, vol. 53(7), p. 287s.
3. C. Chen, A. W. Thompson, and I. M. Bernstein: *Weldments—Physical Metallurgy and Failure Phenomena*, Proceedings, 5th Bolton Landing Conference, R. J. Christoffel, E. F. Nippes, and H. D. Solomon, eds., General Electric Company, Schenectady, NY, 1979, pp. 219-30.
4. J. F. Lesser and W. W. Gerberich: *Metall. Trans. A*, 1976, vol. 7A, p. 953.
5. S. M. Toy and A. Phillips: *Weld. J.*, 1970, vol. 49(11), p. 497s.
6. S. Nagashima, T. Ooka, S. Sekino, H. Mimura, T. Fujishima, S. Yano, and H. Sakurai: *Trans. Iron Steel Inst. Japan*, 1971, vol. 58, p. 402.
7. S. Nagashima, T. Ooka, S. Sekino, H. Mimura, T. Fujishima, S. Yano, and H. Sakurai: *Tetsu-to-Hagané*, 1972, vol. 58, p. 128.
8. J. W. Morris, Jr., C. K. Syn, J. I. Kim, and B. Fultz: *Proceedings, International Conference on Martensitic Transformations*, W. Owen, ed., M.I.T. Press, Cambridge, MA, 1979, pp. 572-77.
9. J. I. Kim and J. W. Morris, Jr.: *Metall. Trans. A*, 1981, vol. 12A, p. 1957.
10. J. I. Kim, C. K. Syn, and J. W. Morris, Jr.: *Metall. Trans. A*, 1983, vol. 14A, p. 93.
11. J. I. Kim, H. J. Kim, and J. W. Morris, Jr.: *Metall. Trans. A*, 1984, vol. 15A, p. 2213.
12. Y. H. Kim and J. W. Morris, Jr.: *Metall. Trans. A*, 1983, vol. 14A, p. 1883.
13. J. I. Kim: Ph.D. Thesis, Dept. Materials Science and Mineral Engineering, University of California, Berkeley, CA, 1979.
14. R. L. Miller: *Trans. ASM*, 1964, vol. 57, p. 892.
15. I. M. Bernstein: *Metall. Trans.*, 1970, vol. 1, p. 3143.
16. H. Haga and H. Mimura: *Trans. Japan Inst. of Metals*, 1972, vol. 13, p. 155.
17. C. K. Syn, B. Fultz, and J. W. Morris, Jr.: *Metall. Trans. A*, 1978, vol. 9A, p. 1635.
18. G. Kurdjumov and G. Sachs: *Z. Physik*, 1930, vol. 64, p. 325.
19. Z. Nishiyama: Sci. Rep. Tohoku Univ., 1934, vol. 23, p. 637.
20. G. Wasserman: *Mitt. K-W-I Eisenforth*, 1935, vol. 17, p. 149.
21. W. W. Gerberich and Y. T. Chen: *Metall. Trans. A*, 1975, vol. 6A, p. 271.
22. C. N. Sastry, K. H. Kahn, and W. E. Wood: *Metall. Trans. A*, 1982, vol. 13A, p. 676.
23. M. Murakami, K. Shibata, and T. Fujita: *Proceedings, International Cryogenic Materials Conference*, Kobe, Japan, K. Tachikawa and A. Clark, eds., Butterworths, London, 1982, p. 356.
24. H. J. Kim, Y.-H. Kim, and J. W. Morris, Jr.: Lawrence Berkeley Laboratory Publication 17617, May 1984, Berkeley, CA, 94720.
25. C. A. Zannis, P. W. Holsberg, and E. C. Dunn, Jr.: *Weld. J.*, 1980, vol. 59(2), p. 355s.